Chapter 2

Atom-photon interactions

2.1 Introduction

As discussed in Sec. 1.1.3.4, the realization of a scalable quantum network based on neutral atoms consisting of $N \gg 1$ quantum nodes requires a significant shift of approach from conventional Fabry-Perot cavity QED systems to a completely different platform in the world of nanophotonics, which utilizes parallel on-chip lithographic fabrication technology. This thesis presents early investigations of this emerging transition, focusing on three specific atom-nanophotonic platforms or systems using microtoroidal resonators, nano-optical fibers, and nanophotonic crystals, all of which involve matter-light interactions at the ~ 100 nm scale.

In this regime of interactions between single atoms and nanophotonics, new issues previously not as significant in conventional cavity QED systems arise, involving, for example, complex electromagnetic field polarizations and atom-surface interaction effects. Although these issues bring about new nontrivial challenges, the prospects are great and these challenges may even turn into opportunities to increase our understanding in this regime, for example through potential precise measurement of Casimir effects by a strongly coupled single-atom probe.

This chapter presents a brief overview of the three specific platforms investigated in this thesis, and introduces the corresponding theoretical models and experimental setups for these systems. Detailed discussions of specific experiments and theoretical studies are included in the subsequent chapters.

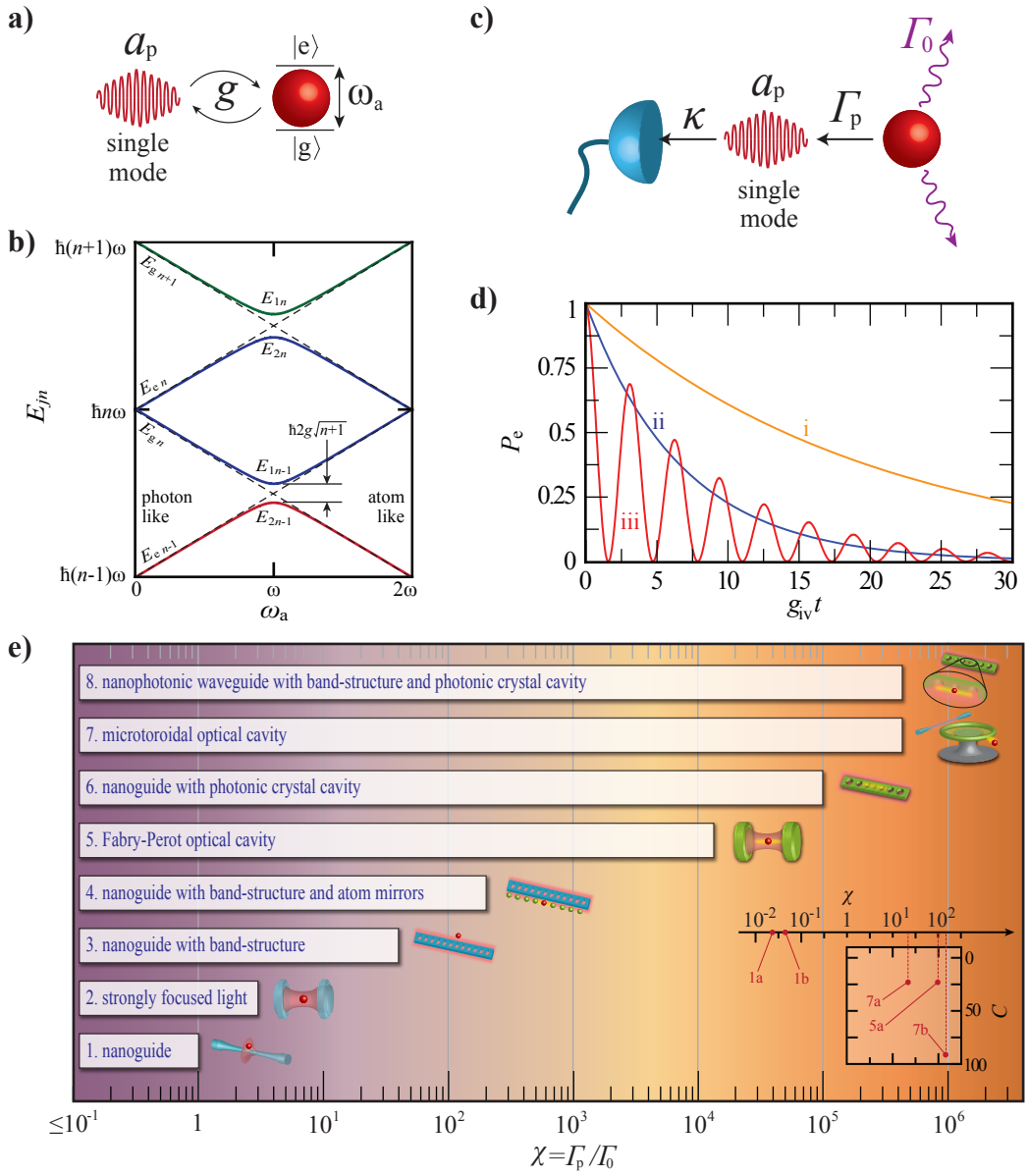

Figure 2.1: **Overview of atom-photon interaction. a)** Two level atom interacting with a single photonic mode a_p at rate g. **b)** Dressed atom energy levels E_{jn} where $j = g, e$ for ground, excited states (dashed lines: absent atom-photon coupling). **c)** Excited atom decay rate into the photonic mode a_p (e.g., waveguide mode, intracavity mode), Γ_p, and decay (loss) rate to the environment, Γ_0. The coupling rate between the mode a_p and detector is κ, which is equal to Γ_p in direct detection, but may be different than Γ_p for a cavity system. **d)** Probability P_e of an initially excited atom to be in the excited state after a time $g_{iv}t$ where $g_{iv} = 105MHz$. (i) Atom free-space decay rate $\Gamma_0/2\pi = 5.2$ MHz. (ii) Enhanced decay rate $\Gamma_p = 2\Gamma_0$. (iii) With $g/2\pi = 105$ MHz, $\kappa/2\pi = 20$ MHz, $\Gamma_0/2\pi = 5.2$ MHz (Cesium D2 line) [5]. **e)** Atom-photon interaction strengths parametrized by $\chi = \Gamma_p/\Gamma_0$ for waveguides 1. to 3. and cavities 4. to 8. Limits are discussed in main text. Inset: Some data points showing χ realized in various experiments, 1a-1b: Nanofiber trap in [248] and [91], also with the corresponding cooperativity parameter C for cavity QED systems with Fabry-Perot (5a) [33], Microtoroid (7a-7b) [9] and [5].

2.2 One atom and a single photonic mode

Consider a simple system that consists of a two-level atom and a single (quantized) electromagnetic field mode as depicted in Fig. 2.1 a). The system is described by the Jaynes-Cummings Hamiltonian that describes the atom-photon interaction by an electric dipole interaction Hamiltonian, $H_{\rm int}$, which is given by the rotating wave approximation [114]:

$$\begin{aligned} H_{\rm tot} &= H_{\rm atom} + H_{\rm photon} + H_{\rm int} && (2.1)\\ &= \frac{1}{2}\hbar\omega_{\rm a}\sigma_z + \hbar\omega a_{\rm p}^{\dagger}a_{\rm p} + \hbar g(a_{\rm p}\sigma^{+} + a_{\rm p}^{\dagger}\sigma^{-}) && (2.2)\end{aligned}$$

where $\sigma^{\pm}$ are Pauli spin-flip operators for the atom, $a_{\rm p}$ is the annihilation operator for the photonic mode of frequency ω, and $H_{\rm int}$ is the interaction Hamiltonian representing absorption of a photon and excitation of the atom from the ground state $|{\rm g}\rangle$ to excited state $|{\rm e}\rangle$ for $(a_{\rm p}\sigma^{+})$ and the converse for $(a_{\rm p}^{\dagger}\sigma^{-})$. The atom-photon coupling strength is given by $\hbar g = \langle\vec{d}\cdot\vec{E}\rangle$, where g is the coupling rate and $\Omega_{\rm R} = 2g$ is the one-photon Rabi frequency. The atomic dipole moment operator is given by $\vec{d} = -e\vec{r} = \vec{d}_{\rm ge}(|{\rm g}\rangle\langle{\rm e}| + |{\rm e}\rangle\langle{\rm g}|)$, where e is the electron's charge, $\vec{r}$ is the relative coordinate core-valence electron, $\vec{d}_{\rm ge}$ is a real numbered vector (not an operator) with direction given by the dipole polarization axis and the magnitude given by the dipole matrix element for the transition between $|{\rm g}\rangle$ and $|{\rm e}\rangle$. The matrix elements $d_{\rm ge}$ can be calculated by using the Wigner-Eckart theorem and Clebsch-Gordan coefficients for the atomic transitions. Note that without loss of generality, we have chosen the matrix element g to be real. Furthermore, since we are considering frequencies close to the atomic resonance, $(\omega - \omega_{\rm a}) \ll \omega_{\rm a}$, we have applied the rotating wave approximation by omitting the terms $a_{\rm p}\sigma^{-}$ and $a_{\rm p}^{\dagger}\sigma^{+}$ as they evolve at optical frequencies $(\omega_{\rm a} + \omega)$.

Solving for the energy eigenstates of the Hamiltonian given in Eq. (2.2) [165], we obtain:

$$E_{1n} = \hbar(n + \frac{1}{2})\omega + \frac{1}{2}\hbar\Omega_{\rm R'} \qquad \text{and} \qquad E_{2n} = \hbar(n + \frac{1}{2})\omega - \frac{1}{2}\hbar\Omega_{\rm R'}, \tag{2.3}$$

where $\Omega_{\rm R'} = \sqrt{\Delta\omega^2 + 4g^2(n+1)}$ is the generalized Rabi flopping frequency, with $\Delta\omega = \omega - \omega_{\rm a}$ the frequency detuning and n the total number of excitations in the system. The eigenenergies of these dressed states are plotted as a function of $\omega_{\rm a}$ for $(n-1), n, (n+1)$ excitations in Fig. 2.1 b). Note the anti-crossings evident on resonant $(\omega_{\rm a} = \omega)$.

Substituting the eigenstates into the Schrödinger equation, we obtain [165] the time-evolution of the dressed state system. For zero initial photon number and a resonant atom initially in the excited

state, the probabilities of exchanging the excitation between the atom and photon mode are:

$$P_{\mathrm{g}}(t) = \sin(gt) \qquad \text{and} \qquad P_{\mathrm{e}}(t) = \cos(gt), \tag{2.4}$$

which show Rabi flopping at the Rabi frequency, due to the vacuum fluctuations in the electromagnetic field, which stimulate an excited atom to emit via a spontaneous emission process.

Although the above simple atom and single photonic mode system is powerful and is intuitive, it is a quite challenging system to realize in practice. This is because, in reality, there are typically numerous modes that all interact with an atom. All of these modes make up a continuous spectrum of vacuum fluctuations that all attempt to make an excited atom Rabi flop. The resulting sum of all of the continuums of probability amplitudes that interfere give rise to the more commonly observed exponential decay of an excited atom by dissipating the energy irreversibly into its environment. The challenge and goal, then, is to realize a system where the coupling strength between the atom and a particularly chosen single photonic mode (e.g., single mode defined by an optical fiber) is much stronger relative to all other dissipative channels such as the vacuum/environment. One of the focuses of this thesis is to investigate and experimentally demonstrate systems that span this coupling strength ratio from small to one of the largest achieved to date. One figure of merit that can be used to compare various systems spanning orders-of-magnitude in coupling strength is the ratio between the atom's decay rate into the single photonic mode, Γ_{p} and the decay rate into all other dissipative modes of the environment, Γ_0, which leads to irreversible loss of information. This ratio,

$$\chi \equiv \Gamma_{\mathrm{p}}/\Gamma_0, \tag{2.5}$$

includes various types of single photonic mode (e.g., optical fiber mode, nano-waveguide mode, optical cavity mode), various types of loss modes (e.g., vacuum, surface modes in cases where the atom is in proximity to a material surface), and various types of enhancements (e.g., ultra-high intensity and small optical mode volume systems, sub-diffraction limit systems, cavity enhancement, and band-structure enhancement). An overview is presented in Fig. 2.1 e) that includes various different platforms discussed in more detail in Sec. 2.5 and the corresponding ranges of the χ parameter. Fig. 2.1 c) shows a general schematic of the systems considered in this thesis, which consist of an atom and a single photonic mode a_{p} that is coupled to the detector at a rate κ. The atom decays into the good single photonic mode at a rate Γ_{p}, and (is lost) into the environment at a rate Γ_0.

In the subsequent chapters, we look at quantitative ways to descibe the system from the weak

coupling regime ($g \ll \kappa, \Gamma_0$) all the way to the strong coupling regime ($g \gg \kappa, \Gamma_0$). Recall that g is the rate of coherent exchange of excitation between an atom and the single mode a_p, with the Rabi flopping frequency $\Omega_\mathrm{R} = 2g$.

2.3 Interaction in the weak coupling regime ($g \ll \kappa, \Gamma_0$)

In Sec. 2.2, we discuss how an initially excited atom Rabi flops purely due to vacuum fluctuations of a single photonic mode. In most realistic cases however, the atom interacts with a continuum of modes of its environment, which leads to an exponential decay of the excited state probability. A simplified but intuitive way to describe this quantitatively is to apply the Fermi Golden Rule (in first order perturbation theory) [165]:

$$\Gamma = \frac{dP_{\mathrm{e}\to\mathrm{g}}}{dt} = 2\pi \frac{|\langle \vec{d}_{\mathrm{ge}} \cdot \vec{E} \rangle|^2}{\hbar^2} \mathscr{D}(\omega) = 2\pi g^2(\omega) \mathscr{D}(\omega), \tag{2.6}$$

where we have used the perturbing Hamiltonian $H_\mathrm{int} = \vec{d} \cdot \vec{E}$ in $g = \frac{\langle \vec{d} \cdot \vec{E} \rangle}{\hbar} = \frac{\langle \vec{d}_{\mathrm{ge}} \cdot \vec{E} \rangle}{\hbar}$, where $\vec{d}_{\mathrm{ge}}$ is the dipole matrix element number with the direction of the atomic dipole polarization. The density of states, $\mathscr{D}(\omega)$, describes the number of final states per unit energy that the atom can decay into (at optical frequency ω), and $P_{\mathrm{e}\to\mathrm{g}}$ is the transition probability from $|\mathrm{e}\rangle$ to $|\mathrm{g}\rangle$.

Although using Fermi's Golden Rule to compute Γ is intuitive and highlights the key factors affecting the decay rate Γ, namely the strength of the coupling g and density of states $\mathscr{D}$, it assumes that the initial atomic state probability remains equal to unity rather than decaying exponentially. Hence it is valid only for times short enough that the excited state population is not significantly depleted [165]. A more general approach is given by the Weisskopf-Wigner theory, which does predict exponential decay of the initial state, and is valid over long time responses. Note that in addition to a decay, the Weisskopf-Wigner theory predicts a frequency shift due to the interaction of the atom with the vacuum fluctuations, known as the Lamb shift. For an atom in free-space, it can be shown [165] that the spontaneous decay rate is given by

$$\Gamma = \frac{\omega_\mathrm{a}^3 d_{\mathrm{ge}}^2}{3\pi\epsilon_0 \hbar c^3} \equiv \gamma_0, \tag{2.7}$$

where ϵ_0 is the vacuum permittivity. This result for free-space spontaneous emission rate of an atom is called Einstein's A coefficient. As discussed previously, the spontaneous emission of an atom is not an intrinsic property but depends on the atom's environment. A nice simple example is a system

that consists of an atom positioned inside an optical cavity with quality factor Q and optical mode volume $V_{\rm m}$. It can be shown that in this case [190]:

$$\frac{\Gamma_{\rm cav}(\omega_{\rm c}=\omega_{\rm a})}{\gamma_0}=F_{\rm p}=\frac{3Q}{4\pi^2}\left(\frac{\lambda^3}{V_{\rm m}}\right), \tag{2.8}$$

where on resonance (cavity resonance frequency $\omega_{\rm c}$ is equal to atomic transition frequency $\omega_{\rm a}$), we see enhancement of spontaneous decay rate by the Purcell factor ($F_{\rm p}$), $\Gamma_{\rm cav}/\gamma_0=F_{\rm p}$, as the density of state is enhanced by the cavity —the Purcell effect [190]. Note that an implicit assumption in the above equations is that the material presence of the cavity does not alter the atom's electronic states and dissipative decay rates γ_0. As we will discuss in later sections, this assumption may break down in nanophotonics, where the atom's proximity to material surfaces can be sufficiently close that the dissipative decay rates can be modified say by the presence of surface modes, and the internal state of the atoms may be affected by Casimir effects between the atom and material surfaces. In this case, the free space decay rate γ_0 becomes Γ_0, which may be larger or smaller than γ_0 depending on the surrounding environment. We note that this effect of modification to γ_0 involves multi-level atom description. In addition to enhancement of atom spontaneous emission, inhibition can also occur when the density of states that the atom can decay into is suppressed by the cavity, for example, if the lowest electromagnetic field frequency supported by the cavity is higher than the atom's transition frequency. Inhibited spontaneous emissions[1] were first demonstrated in 1974 by Drexhage [70], and in the 1980s by Kleppner [137, 109] and Gabrielse [84]. Enhanced atomic spontaneous emission in a resonant cavity was first observed in Rydberg atoms of sodium by Haroche [94, 195].

Treating a two-level atom in a cavity with Γ_0 (atom's spontaneous decay rate in its specific surrounding environment) and κ (cavity decay rate), we can describe the dissipative system by using the master equation [23] (at zero temperature):

$$\frac{\partial}{\partial t}\rho=-i\hbar[H_{\rm tot},\rho]-\frac{\Gamma_0}{2}[\sigma^+\sigma^-\rho(t)+\rho(t)\sigma^+\sigma^--2\sigma^-\rho(t)\sigma^+]-\frac{\kappa}{2}[a^+a\rho(t)+\rho(t)a^+a-2a\rho(t)a^+], \tag{2.9}$$

where $H_{\rm tot}$ is given by Eq. (2.2), Γ_0 is the coupling of the atom to the environment (loss channels),

[1] Drexhage et al. in 1974 studied the fluorescence of a dye film on a mirror and observed an alteration of the fluorescence lifetime arising from the interference of the molecular radiation with its surface image [70]. Large inhibition of spontaneous emission was first clearly observed by Gabrielse and Dehmelt where a single electron confined in a Penning trap was shown to have a lifetime up to ten times longer due to inhibition of spontaneous emission by the cavity formed by the electrodes [84]. In the experiment by Kleppner et al., Rydberg atoms were placed between two parallel conducting plates that led to a longer excited state lifetime by a factor of 20 due to inhibited spontaneous emissions by the cavity [109].

and κ is the coupling of the system into the output mode (detector) as illustrated in Fig. 2.1 c). In this case, the general solution [23] for the probability amplitude of the atom in the excited state is given by:

$$c_{\mathrm{e}}(t) = c_{\mathrm{e}1}e^{\alpha_1 t} + c_{\mathrm{e}2}e^{\alpha_2 t}, \tag{2.10}$$

where

$$\alpha_{1,2} = -\frac{1}{2}\left(\frac{\Gamma_0}{2} + \frac{\kappa}{2} + i\Delta\omega\right) \pm \frac{1}{2}\left[\left(\frac{\Gamma_0}{2} + \frac{\kappa}{2} + i\Delta\omega\right)^2 - 4g^2\right]^{1/2}, \tag{2.11}$$

with some coefficients $c_{\mathrm{e}1}$ and $c_{\mathrm{e}2}$. The probability for the atom in the excited state is given by $P_{\mathrm{e}}(t) = |c_{\mathrm{e}}(t)|^2$. A few example cases that illustrate the behaviour of $P_{\mathrm{e}}(t)$ based on Eq. (2.10) are shown in Fig. 2.1 d) showing free-space cesium atom exponential decay ($c_{\mathrm{e}1} = 0, c_{\mathrm{e}2} = 1, \Gamma_0 = \gamma_0 = 5.2\mathrm{MHz}, \kappa = 0$) in i, and with $\kappa = \Gamma_{\mathrm{p}} = 2\Gamma_0$ in ii, the rest of parameters being the same as in i. In the second case, ii, the decay rate is dominated by κ which in this case is set to $\Gamma_{\mathrm{p}} = 2\Gamma_0$. This illustrates the enhancement of the decay rate into a single photonic mode, resulting in a total atom decay rate of $\Gamma_{\mathrm{tot}} = 3\Gamma_0$. In these cases, we have assumed the weak coupling regime, $g \ll \kappa, \Gamma_0$. The case for the strong coupling regime where $g \gg \kappa, \Gamma_0$ is discussed in the next section.

2.4 Interaction in the strong coupling regime ($g \gg \kappa, \Gamma_0$)

In the strong coupling regime where $g \gg \kappa, \Gamma_0$, Eq. (2.11) reduces to

$$\alpha_{1,2} = -\frac{1}{2}\left(\frac{\Gamma_0}{2} + \frac{\kappa}{2} + i\Delta\omega\right) \pm ig, \tag{2.12}$$

which leads to a damped oscillation of $P_{\mathrm{e}}(t)$ with the Rabi frequency $\Omega_{\mathrm{R}} = 2g$ with a damping constant $(\Gamma_0 + \kappa)/4$. Some example cases of $P_{\mathrm{e}}(t)$ are shown in Fig. 2.1 d), iii, for a cesium atom coupled to a microtoroidal resonator using the experimental parameters discussed in Chapter 5 of this thesis ($c_{\mathrm{e}1} = c_{\mathrm{e}2} = 0.5, g = 105\mathrm{MHz}, \kappa = 20\mathrm{MHz}, \Gamma_0 = 5.2\mathrm{MHz}$). This corresponds to a cesium atom located at about 100nm from the surface of the microtoroid.

As discussed in Sec. 2.2, the realization of atom-photon interaction in the strong coupling regime requires a strong enhancement in the density of states for an atom to decay into the photonic (single) mode, relative to all other dissipative channels into the environment. One powerful technique to realize such a system is to use a high quality optical resonator, where an atom can be coupled to the photonic cavity mode much more strongly than the coupling to its environment. In the subsequent sections below, we discuss in more detail the qualities and relevant figure of merits, firstly of an

optical cavity, and secondly in connection to the strength of atom-photon interaction.

2.4.1 Optical cavity

An optical cavity can be thought of as a photonic trap, where, upon entering a cavity, an input photon gets 'trapped' within the electromagnetic mode volume of the cavity, as it bounces around inside the cavity for a large number of times before it can escape out of the cavity. Some examples of optical cavities are illustrated in Fig. 2.3. As more photons enter the cavity as the intracavity photons are bouncing around, the intracavity power continually build up until it reaches an equilibrium, where in this steady-state condition, the rate of increase in intracavity power due to new incoming photons, equals the rate of energy dissipation due to intracavity losses such as material absorption or radiative loss, and outcoupling of the intracavity photons as they escape the cavity. We will now proceed to describe the aforementioned mathematically.

Two figure of merits of an optical cavity are its finesse, $\mathscr{F}$ and quality factor, Q. The cavity finesse is the number of bounces an intracavity photon will make before its probability of escaping the cavity are $1/e$. It is a measure of how small the total losses of the cavity is (both due to intrinsic losses such as absorption and radiative loss, as well as extrinsic coupling to the input/output port). The cavity finesse is related to the cavity free spectral range wavelength and angular frequency, $\Delta\lambda_{\mathrm{FSR}}$ and $\Delta\omega_{\mathrm{FSR}}$, and the full-width-half-maximum, $\delta\lambda_{\mathrm{fwhm}}$ and $\delta\omega_{\mathrm{fwhm}}$ by:

$$\mathscr{F} = \frac{\Delta\lambda_{\mathrm{FSR}}}{\delta\lambda_{\mathrm{fwhm}}} = \frac{\Delta\omega_{\mathrm{FSR}}}{\delta\omega_{\mathrm{fwhm}}}. \tag{2.13}$$

In contrast to the cavity finesse ($\mathscr{F}$) which is independent from the cavity length, the cavity quality factor (Q) depends on the cavity length, L_{cav}. This is because the quality factor measures the cavity's ability to store energy. It is equal to 2π times the ratio of stored intracavity energy to the energy loss per oscillation cycle. Here, an oscillation cycle refers to the field oscillation cycle, not the cavity round-trip cycle. The cavity quality factor Q is given by:

$$Q = \mathscr{F}\frac{n_{\mathrm{cav}}L_{\mathrm{cav}}}{\lambda_{\mathrm{cav}}} = \frac{\omega_{\mathrm{cav}}}{\delta\omega_{\mathrm{fwhm}}} = \frac{\lambda_{\mathrm{cav}}}{\delta\lambda_{\mathrm{fwhm}}} = \omega_{\mathrm{cav}}\tau, \tag{2.14}$$

where ω_{cav} and λ_{cav} are the resonant angular frequency and wavelength of the cavity mode respectively ($\omega = 2\pi c/\lambda$), for optical frequency ν), n_{cav} is the refractive index of the cavity medium and L_{cav} is the total round-trip cavity length. For example, L_{cav} is equal to twice the physical linear length of a Fabry-Perot cavity, and it is equal to the effective circumference of a microtoroidal cavity.

The cavity lifetime, τ, describes the $1/e$ decay time of the cavity photons. For example, for a cavity with initial N_0 number of photons, the number of photons after time t is given by $N(t) = N_0 e^{-t/\tau}$. The free spectral range and full width half maximum quantities are given by:

$$\Delta\lambda_{\mathrm{FSR}} = \frac{\lambda_{\mathrm{cav}}^2}{n_{\mathrm{cav}} L_{\mathrm{cav}}}, \qquad \Delta\omega_{\mathrm{FSR}} = \frac{c}{n_{\mathrm{cav}} L_{\mathrm{cav}}} \tag{2.15}$$

$$\delta\omega_{\mathrm{fwhm}} = 2\kappa, \qquad \delta\lambda_{\mathrm{fwhm}} = \frac{\lambda_{\mathrm{cav}}^2}{c} 2\pi\delta\omega_{\mathrm{fwhm}}, \tag{2.16}$$

where c is the speed of light in vacuum, and where we have used first-order Taylor expansion $d\lambda = \frac{c}{f^2} df = \frac{\lambda^2}{c} df$. Note that the cavity lifetime τ is related to the linewidth by $\tau = Q/\omega = 1/(2\kappa)$. The quantity κ represents the total decay rate of the cavity field amplitude. It can be decomposed into intrinsic and extrinsic loss rates as $\kappa = \kappa_{\mathrm{i}} + \kappa_{\mathrm{ex}}$, where intrinsic losses include material and defects absorption and radiative losses, and extrinsic loss is given by the coupling rate of the cavity to the input/output optical port. Correspondingly, we can define intrinsic and extrinsic quality factors:

$$\kappa = \frac{\pi c}{\lambda_{\mathrm{cav}} Q}, \qquad \kappa_{\mathrm{i}} = \frac{\pi c}{\lambda_{\mathrm{cav}} Q_{\mathrm{i}}}, \qquad \kappa_{\mathrm{ex}} = \frac{\pi c}{\lambda_{\mathrm{cav}} Q_{\mathrm{ex}}}, \tag{2.17}$$

where Q is the total quality factor, and Q_{i} and Q_{ex} are the intrinsic and extrinsic quality factors. Note that ω and κ have angular frequency units.

With the above parameters, we now look at the cavity power build up factor, which is the ratio of the intracavity circulating power (P_{circ}) to the input power (P_{in}). An approximate solution is simply given by $P_{\mathrm{circ}}/P_{\mathrm{in}} = \mathscr{F}/\pi$, where $\mathscr{F}$ is the cavity finesse. The exact solution is given by [134]:

$$\frac{P_{\mathrm{circ}}}{P_{\mathrm{in}}} = \frac{c\Delta\lambda_{\mathrm{FSR}}}{\lambda_{\mathrm{cav}}^2} \frac{1}{\tau_{\mathrm{ex}}} \left(\frac{1}{2\tau_{\mathrm{i}}} + \frac{1}{2\tau_{\mathrm{ex}}} \right)^{-2} = \frac{2\lambda_{\mathrm{cav}}}{\pi n_{\mathrm{cav}} L_{\mathrm{cav}}} Q_{\mathrm{ex}} \left(1 + Q_{\mathrm{ex}}/Q_{\mathrm{i}}\right)^{-2}. \tag{2.18}$$

2.4.2 Cavity QED

In the previous section, we discussed the parameters that are important in determining the performance of an optical cavity. In this section, we consider placing a single atom inside the electromagnetic field mode volume of an optical cavity, and discuss the various parameters that are important in characterizing the performance of such a cavity QED system. There are four critical parameters that determine the nature of atom-photon interactions in a cavity QED setting. Firstly, we consider the number of times an intracavity photon bounces around and hence interact with a single atom. This is given by the finesse of the cavity, $\mathscr{F}$, which is proportional to the quality factor Q according to Eq. (2.14). The larger the Q is, the stronger the atom-photon interaction will be. Secondly, the

strength of atom-photon interaction is determined by the energy density associated with a single photon distributed within the cavity's mode volume, V_{m}. The smaller the mode volume V_{m} is, the stronger the interaction between a single atom and a single photon will be. Thirdly, in realistic cavities, there are are some distributions of electric field strength within the mode volume of the cavity. For example, in a Fabry-Perot cavity like one shown in Fig. 2.3 a), the electric field strength $|\vec{E}(\vec{r_{\mathrm{a}}})|$ varies as a function of space. In the transverse direction, depending on the atom's position $\vec{r_{\mathrm{a}}}$, the electric field strength varies from a small value at the tail of the Gaussian intensity profile, to a maximum at the center of the Gaussian intensity profile. Along the longitudinal direction, it varies from zero at the nodes of the standing-wave and maximum at the antinodes. This behavior is quantitatively specified by the ratio $|\vec{E}(\vec{r_{\mathrm{a}}})|/|\vec{E}_{\mathrm{max}}|$. The larger this ratio is, the stronger the atom-photon interaction will be. Fourthly, we consider the size of the atomic dipole moment. The larger the value of the dipole moment, the stronger the interaction between the atomic dipole and the electromagnetic field, as expected.

As discussed previously in this chapter, the strength of atom-photon interaction is quantitatively described by the coupling parameter g, which is directly related to the Rabi flopping rate $\Omega_{\mathrm{R}} = 2g$ that represents the frequency at which an excitation is exchanged between a single atom and the photonic mode of the cavity. This coupling strength parameter g is given by [224]:

$$g(\vec{r_{\mathrm{a}}}) = \Gamma_{0\perp}(\vec{r_{\mathrm{a}}})|\vec{E}(\vec{r_{\mathrm{a}}})/\vec{E}_{\mathrm{max}}|\sqrt{V_{\mathrm{a}}(\vec{r_{\mathrm{a}}})/V_{\mathrm{m}}}, \tag{2.19}$$

where $\Gamma_{0\perp}(\vec{r_{\mathrm{a}}})$ is the atom transverse decay rate into all other channels other than the cavity mode that may depend on the atom's position $\vec{r_{\mathrm{a}}}$. The transverse decay rate is given by $\Gamma_{0\perp}(\vec{r_{\mathrm{a}}}) \geq \Gamma_0(\vec{r_{\mathrm{a}}})/2$ where $\Gamma_0(\vec{r_{\mathrm{a}}}) = \Gamma_{0\parallel}(\vec{r_{\mathrm{a}}})$ is the spontaneous decay rate into the environment, also known as the longitudinal decay rate [227]. This is because $\Gamma_0 = \Gamma_{0\parallel}$ is the rate of relaxation of the z-component of the Bloch vector to the ground state, whereas $\Gamma_{0\perp}$ is the rate at which coherences damp, which is damping in the direction transverse to the z-axis of the Bloch vector. Note that the longitudinal relaxation time (from excited to ground state) is given by $T_1 = 1/\Gamma_0$ and the transverse relaxation (dephasing) time $T_2 = 1/\Gamma_{0\perp}$. For a cesium D2 line in vacuum (free-space), $\Gamma_{0\perp}/2\pi = \gamma_{0\perp}/2\pi =$ 2.61 MHz. Note that γ_0 represents the decay rate in vacuum (free-space), while Γ_0 represents the decay rate into the environment given the atom's specific position and surrounding, which may be larger or smaller than γ_0. For example, if the atom is in close proximity to a dielectric surface, Γ_0 may be larger than γ_0 because of the increased density of states that the atom can decay into, such as into the surface modes of the dielectric. The other terms in Eq. (2.19) are $|\vec{E}(\vec{r_{\mathrm{a}}})|$, the electric field

strength at $\vec{r}_{\rm a}$, $|\vec{E}_{\rm max}|$, the maximum electric field strength of the cavity mode, $V_{\rm a}$, the characteristic atomic interaction volume, and $V_{\rm m}$, the cavity electromagnetic mode volume, given by:

$$V_{\rm a}(\vec{r}_{\rm a}) = \frac{3c\lambda_{\rm a}^2}{4\pi\Gamma_{0\perp}(\vec{r}_{\rm a})}, \qquad V_{\rm m} \equiv \frac{\int_{V_{\rm Q}} \epsilon(\vec{r}_{\rm a})|\vec{E}(\vec{r}_{\rm a})|^2 d^3\vec{r}_{\rm a}}{|\vec{E}_{\rm max}|^2}, \tag{2.20}$$

where $V_{\rm Q}$ represents a quantization volume of the electromagnetic field and $\epsilon(\vec{r}_{\rm a}) = (n(\vec{r}_{\rm a}))^2$ is the relative permittivity, which is the square of the refractive index at $\vec{r}_{\rm a}$.

Taking into account the decay or dissipative rate of the cavity, $\kappa = \kappa_{\rm i} + \kappa_{\rm ex}$, another important parameter that describes the strength of atom-photon interaction in the cQED setting (relative to the loss channels), is the so-called cooperativity parameter, C, which is given by:

$$C(\vec{r}_{\rm a}) = \frac{g(\vec{r}_{\rm a})^2}{2\kappa\Gamma_{0\perp}(\vec{r}_{\rm a})} = \frac{3\lambda_{\rm a}^3|\vec{E}(\vec{r}_{\rm a})/\vec{E}_{\rm max}|^2}{8\pi^2}\frac{Q}{V_{\rm m}}, \tag{2.21}$$

where we note that $C \sim |\vec{E}(\vec{r}_{\rm a})/\vec{E}_{\rm max}|^2 Q/V_{\rm m}$. The enhancement of the atomic decay rate into the cavity mode is given by the Purcell factor, $P_{\rm F} = 1 + 2C = \Gamma_{\rm p}/\Gamma'_{\rm p}$, where $\Gamma'_{\rm p}$ is the decay rate without the cavity enhancement. For example, consider an atom in free-space with a decay rate of $\Gamma_0 = \gamma_0$. Placing a relatively macroscopic Fabry-Perot cavity surrounding it, that lead to a cooperativity parameter of $C = 10$, will enhance the decay rate into the cavity mode to be $\Gamma_{\rm p} = P_{\rm F}\Gamma_0 = 21\Gamma_0 = 21\gamma_0$. As another example, consider an atom located in close proximity to an optical nanofiber waveguide, which is coupled to the waveguide through the sub-wavelength evanescent field surrounding the single-mode nanofiber. Without a cavity, the decay rate into the environment is enhanced due to the presence of the dielectric surface, for example $\Gamma_0 \approx 1.5\gamma_0$. Now because of the strong intensity of the nanofiber mode (i.e., the small effective area $A_{\rm eff}$ defined below), then the scattering rate $R_{\rm sc} \sim \sigma/A_{\rm eff}$ becomes large and leads to an enhanced decay rate into the nanofiber mode, say $\Gamma_{\rm p} = 0.2\Gamma_0$. In addition to all of these, suppose we add a pair of mirrors on both ends of the nanofiber, forming a cavity, which leads to a cooperativity parameter of $C = 10$. Then, for this nanofiber cQED system, the decay rate into the cavity mode will be $\Gamma_{\rm p} = P_{\rm F}\Gamma'_{\rm p} = (21)(1 + 0.2)\Gamma_0 = (21)(1.2)(1.5\gamma_0) = 37.8\gamma_0$.

The electromagnetic field effective area $A_{\rm eff}$ is defined by

$$A_{\rm eff} = A_{\rm eff}(\vec{r}) = \frac{P}{I(\vec{r})}, \tag{2.22}$$

where $I(\vec{r})$ is the electric field intensity at location $\vec{r}$, and P is the propagating optical power in

the direction of light propagation. For example, in a nanofiber, P is the optical power propagating along the fiber axis, it does not include contributions from the transverse components of the Poynting vector. This propagating power P is equal to the optical power measurable at the output of the fiber, $P = P_{\text{out}}$.

Two important figure of merits that describe a cavity QED system are the critical photon number, n_0, and critical atom number, N_0. The critical photon number corresponds to the number of photons required to saturate an intracavity photon, while the critical atom number corresponds to the number of atoms required to have an appreciable effect on the intracavity field. They are given by [224]:

$$n_0 = \frac{\Gamma_{0\perp}^2}{2g^2}, \qquad N_0 = \frac{2\Gamma_{0\perp}\kappa}{g^2} = \frac{1}{C}, \tag{2.23}$$

where the dependence of the quantities on the atom's location $\vec{r}_{\text{a}}$ is implicitly assumed, and C is the cooperativity parameter. In cQED systems with strong atom-photon couplings, these numbers can be very small. For example, for a microtoroidal cavity QED systems, they can take the values of $n_0 \sim 10^{-3} - 10^{-5}$ photons and $N_0 \sim 10^{-2} - 10^{-7}$ atoms.

Finally, we note that in cavity QED systems in weak to intermediate coupling, the Purcell factor is an especially important parameter that measures the strength of the atom-photon interaction, where the coupling strength increases with increasing P_{F}. In the strong coupling regime, the condition requirement is more strict, and the important parameter is the coupling rate g, which is compared to all other dissipative rates κ and Γ_0. The criterion for strong coupling regime is

$$g \gg \kappa, \Gamma_0. \tag{2.24}$$

Here, the coherent Rabi flopping process of excitation exchange between a single atom and the cavity field mode dominates over all other dissipative processes, including losses of information by decay processes into the environment, by absorption of materials and defects, and by the coupling into the input/output port of the cavity. In this case, the time evolution of the system involves oscillations in the atomic excited state probability at the Rabi flopping frequency Ω_{R} as shown in Fig. 2.1 d) curves iii and iv.

2.5 Platforms for atom-photon interactions

In this section, we present an overview of various atom-photon interaction platforms, including the platforms specifically investigated in this thesis, namely microtoroidal cavity QED, optical nanofiber, and nanophotonic waveguides and cavities. As with Sec. 2.1 and Fig. 2.1 e), the idea is to give a broad perspective comparing the range of atom-photon interaction strengths and the benefits, disadvantages, challenges and limitations of the various types of platforms, which span orders of magnitudes. As such, the emphasis here is more on the qualitative behavior and features of the types of platforms, the key factors involved in each type, and rough or order of magnitude comparisons, instead of precise quantitative investigations, which will be discussed in more detail in the subsequent chapters.

The basic diagram of the system is shown in Fig. 2.2 a), and consists of a single (two-level) atom with transition frequency ω_{a} between the ground ($|\mathrm{g}\rangle$) and excited ($|\mathrm{e}\rangle$) states, which interacts with a single photonic mode a_{p}. Note that, more precisely, it consists of four modes, two forward- and backward-propagating modes at the input side and two forward- and backward-propagating modes at the output side. For a single sided excitation (from the input side), this leads to two measurable quantities, namely transmission (of the input light after interaction with an atom) and reflection (of the input light after interaction with an atom). For an input power P_{in}, it corresponds to the transmitted power P_{T} and reflected power P_{R}, where $P_{\mathrm{in}} = P_{\mathrm{T}} + P_{\mathrm{R}} + P_0$, and P_0 is the power loss into the environment. The decay rate of an excited atom into the photonic mode is Γ_{p}, symmetrically going into the forward and backward directions, each at a rate of $\Gamma_{\mathrm{p}}/2$. The decay rate of the atom into all other channels other than this photonic mode (i.e., into the environment), is given by Γ_0, which may be different than the free-space decay rate γ_0 depending on the atom's environment. As discussed in Sec. 2.1, in an isolated single atom and single photonic mode coherent system absent of any dissipations, the system is described by the Jaynes-Cummings Hamiltonian, which leads to Rabi flopping oscillations at the Rabi frequency $\Omega_{\mathrm{R}} = 2g$. In most realistic systems such as in free-space or with nanophotonic waveguides (with the exception of strong coupling systems such as in certain cavity QED systems), there exists a continuum of modes whereby all of the probability amplitudes, each undergoing Rabi flopping, destructively interfere, and lead to an exponential decay behavior, with the $1/e$ lifetime given by $1/\Gamma_{\mathrm{p}}$ and $1/\Gamma_0$. For example, for the cesium D2 line, the free-space natural linewidth is $\Gamma_0/2\pi = \gamma_0/2\pi = 5.2$ MHz, and the lifetime is 30.5 ns.

As illustrated in Fig. 2.2 a), in the weak coupling regime, where the atom decays exponentially at some enhanced rate $\Gamma_{\mathrm{tot}} = \Gamma_{\mathrm{p}} + \Gamma_0$, a measure of the strength of the atom-photon coupling into

the photonic mode a_p is $\chi = \Gamma_\mathrm{p}/\Gamma_0$, which is determined by the electric field $E(\omega_\mathrm{p})$ at the frequency ω_p and the electric dipole moment of the atom d_ge between the two states $|\mathrm{g}\rangle$ and $|\mathrm{e}\rangle$. In the strong coupling regime, where the atom decays with Rabi oscillations resembling the pure Jaynes-Cummings system, one could start modeling the system using the Jaynes-Cummings interaction Hamiltonian H_int as given by Eq. (2.2), and including the relatively weak dissipations in the system using techniques such as the master equation in Eq. (2.9). Here, the strength of the interaction is more conveniently characterized by the coupling parameter g, which is related to the Rabi frequency by $\Omega_\mathrm{R} = 2g$.

In this section, we will first look at various platforms that do not involve any optical cavity, which are mostly in the weak coupling regime. Here, we characterize the strength of atom-photon interactions by the parameters Γ_p, and $\chi = \Gamma_\mathrm{p}/\Gamma_0$, transmittance $T = P_\mathrm{T}/P_\mathrm{in}$, and reflectance $R = P_\mathrm{R}/P_\mathrm{in}$. In the second subsection, we will look at various platforms that involve optical cavities, which are mostly in the strong coupling regime. Here, we characterize the strength of atom-photon interactions by the parameter g, which is related to the cooperativity parameter by $C = g^2/2\kappa\Gamma_{0\perp}$ as given by Eq. (2.21), as well as by the parameter $\chi = \Gamma_\mathrm{p}/\Gamma_0$, where Γ_p represents the atomic decay rate into the cavity mode a_p. Finally, in Fig. 2.1 e) we compare all of the platforms considered, from the weak to strong coupling regimes, by the single parameter $\chi = \Gamma_\mathrm{p}/\Gamma_0$.

2.5.1 Atom-photon interactions without a cavity

2.5.1.1 Free-space

We start by considering a very simple scenario of shining a collimated laser beam, say with a beam radius of 1 mm, onto a single atom hypothetically held fixed in free-space. For simplicity, let us assume that the laser power is very weak such that it is far below the intensity saturation threshold of the single atom, and that the laser frequency is resonant to the atomic transition frequency. We then ask the question: What fraction of power of the laser beam will be scattered by the single atom? The answer to this is given by the ratio of the atom's absorption cross-section area to the beam's cross-section area, the scattering ratio given by

$$R_\mathrm{sc} \equiv \frac{P_\mathrm{out}}{P_\mathrm{in}} \approx \frac{\sigma_0}{A_\mathrm{eff}}, \tag{2.25}$$

where $\sigma_0 = \frac{3\lambda^2}{2\pi}$ is the atom's free-space resonant absorption cross-section area (that can be interpreted as the effective area of the atom for removing radiation from the incident light beam), and

$A_{\text{eff}} = \pi w^2/2$ is a Gaussian beam's cross-sectional area, where w = Gaussian beam $1/e$ radius. For cesium D2 line ($\lambda = 852$ nm) and $\sigma_0 \approx 0.35\ \mu\text{m}^2$. For our hypothetical example with $w = 1$ mm, A_{eff} = 1.6 mm^2, and the scattering ratio $R_{\text{sc}} \approx 2.2 \times 10^{-7}$, the answer to our question is essentially zero. As evident from Eq. (2.25), an appreciable scattering ratio can only be achieved with $A_{\text{eff}} \sim \lambda^2 \sim 1$ μm^2.

In the spirit of increasing free-space incident light beam intensity, or in other words, decreasing A_{eff}, let us now consider a system consisting of a pair of two focusing lenses with focal length f as illustrated in Fig. 2.2 c), where a collimated beam, say out of a single-mode fiber, can enter the lens from the left hand side P_{in}, focus down after a distance of approximately f, interact with an atom at this location, diverge and get collimated by the second lens, and couple back into a single-mode fiber, P_{out}. Although this technique significantly increases the atom-photon interaction strength, there are fundamental limits to the inverse, due to two main reasons. Firstly, there is a limit to how much light can be focused, the diffraction limit, $D_{\text{beam}} \sim \lambda/2$, where D_{beam} is the beam's diameter. Secondly, as one confines the light beam (propagating electromagnetic field) into a very small space, complex polarization structure emerges, which results, for example, in a significant electric field component parallel to the wavevector of the beam. Because of these reasons, simple paraxial approximation approaches of focusing light to a very high degree break down in this regime, and a more involved model describing the system is required. This problem was first investigated in 2000 [243] and had been investigated further experimentally in 2008 [233, 234], where the record light absorption by a single Rubidium-87 atom trapped at the center between the pair of lenses is about 10%, that is, a single atom transmittance of $T = 0.90$. Here, the probe light's waist size is $w \approx 800$ nm and λ = 780 nm.

For a system consisting of a single-mode input fiber, a pair of focusing lenses, and an output single-mode fiber, as illustrated in Fig. 2.2 c), the scattering rate R_{sc} is given by [234]:

$$R_{\text{sc}} = \frac{3}{4u^3} e^{2/u^2} \left[\Gamma_{\text{fn}}\left(-\frac{1}{4}, \frac{1}{u^2}\right) + u\Gamma_{\text{fn}}\left(\frac{1}{4}, \frac{1}{u^2}\right) \right]^2, \tag{2.26}$$

where $\Gamma_{\text{fn}}(a, b) = \int_b^\infty t^{a-1} e^{-t} \text{d}t$ is the gamma function, $u = w_{\text{in}}/f$ is the focusing strength parameter, w_{in} is the input collimated beam's Gaussian $1/e$ beam radius (waist) and f is the focal length of each of the two lenses. The transmission into the single-mode fiber at the output side, $T = P_{\text{T}}/P_{\text{in}}$, and reflection back into the single-mode fiber at the input side, $R = P_{\text{R}}/P_{\text{in}}$ are given by [234]:

$$T = (1 - R_{\text{sc}}/2)^2, \qquad R = R_{\text{sc}}^2/4, \tag{2.27}$$

where R_{sc} is given by Eq. (2.26), and the fraction of power lost or scattered into the environment is given by $T_0 = P_0/P_{\mathrm{in}} = 1 - T - R$ where P_0 is the amount of power lost into the environment. We note that the emission of the atom is symmetric into the forward-propagating mode and backward-propagating mode, such that the fraction of power emitted into the single-mode fiber (in both directions) is equal to $2R$. Now the ratio of the decay rate of the atom into the photonic mode (that is into both the forward and backward directions of the single-mode fibers), Γ_{p}, to the decay rate into the environment, Γ_0, is given by:

$$\chi = \frac{\Gamma_{\mathrm{p}}}{\Gamma_0} = \frac{2P_{\mathrm{R}}}{P_0} = \frac{2R}{1-T-R} = \frac{2R}{T_0}. \tag{2.28}$$

The results for T, R, χ, along with the corresponding result for paraxial approximation χ', using paraxial approximation scattering rate $R'_{\mathrm{sc}} = 3u^2$ are shown in Fig. 2.2 d). We see that the highest possible value for χ is $\chi_{\mathrm{max}} = \chi(u = 2.24) = 2.7$ at $u = 2.24$. The record experimental result demonstrated in [233] is shown in Fig. 2.2 d) at point (i), with $u = 0.31$ and $T = 1 - 0.104$. This was achieved using an incident 'collimated' probe beam ($\lambda = 780$ nm) of radius $w_{\mathrm{in}} = 1.4$ mm, focused down to $w_{\mathrm{f}} = 800$ nm. The discrepancy from the theoretical prediction of $T_{\mathrm{pred}} = 1 - 0.2299$ is attributed to non-ideality of the lenses used and reduction of the interaction strength due to the motion of the atom in the dipole trap formed at the focus of the pair of lenses, which has an estimated temperature of ~ 100 μK [233].

2.5.1.2 Nanophotonic waveguides

In Sec. 2.5.1.1, we discussed reducing the effective photonic mode area, A_{eff} by using an increasingly strong focusing parameter u, to increase the atom-photon interaction strength. We noted that one of the ultimate limits of this approach is the diffraction limit $D_{\mathrm{beam}} \sim \lambda/2$, where D_{beam} is the beam's spot size diameter. In this section, we explore platforms based on nanophotonic waveguides such as an optical nanofiber, a nanobeam, or a nanobeam with periodic structure forming a photonic crystal, where an atom can interact with evanescent fields of the modes that are sub-diffraction-limited. This allows for potentially stronger interactions than those possible in the free-space systems discussed in Sec. 2.5.1.1.

A nanophotonic waveguide system using a tapered optical nanofiber is illustrated in Fig. 2.2 e), and one using a nanobeam (without or potentially with periodic structure forming a photonic crystal) in Fig. 2.2 f). As in Sec. 2.5.1.1, an atom now coupled to the evanescent fields of the single-mode nano-waveguides can absorb an incident photon and emit back into the nanoguide mode at a rate of

$\Gamma_p/2$ in the forward direction, and $\Gamma_p/2$ into the backward direction, and it can also emit into the environment at a rate of Γ_0. Also as discussed in Sec. 2.5.1.1, the atom-photon coupling strength affects the transmittance $T = P_T/P_{in}$, reflectance $R = P_R/P_{in}$, and power fraction lost into the environment $T_0 = P_0/P_{in}$ for a given incident input power P_{in}. We note that $P_T = \hbar\omega_a\Gamma_p/2$, $P_R = \hbar\omega_a\Gamma_p/2$, and $P_0 = \hbar\omega_a\Gamma_0$, and $T + R + T_0 = 1$ by conservation of energy. We should stress that in these types of systems, the important parameters involve all of T, R, T_0 (three parameters), not just one scattering ratio parameter $R_{sc} = P_{out}/P_{in}$ as in the case of simple (weak) free-space interaction between a beam of light and atoms, because while in such cases it is implicitly assumed that any light absorbed by the atom will be lost (scattered) into the environment, in more strongly coupled systems such as these nanoguide systems, the emission from the atom may go into the nanoguide's mode with non-negligible probability.

Now consider a silica optical nanofiber system with fiber radius $a = 200$ nm. Here, there are multiple factors that are important in determining the dynamics and strengths of atom-photon coupling for an atom located in close proximity to the nanofiber, overlaping with the evanescent field of the nanoguide. Firstly, due to the strong transverse confinement of the fiber mode field, a high intensity (small A_{eff}) can be achieved, increasing the strength of atom-photon interaction. Secondly, the significant longitudinal component of the electric field of the fiber mode leads to a transverse component of the Poynting vector, which interacts with the atom. Thirdly, the presence of the dielectric surface of the nanofiber modifies the spontaneous emission rate of the atom, $\Gamma_0 \neq \gamma_0$ (see Fig. 5.1 (c) (iii)). And finally, the multilevel structure of a real atom also needs to be taken into account. All of these aspects, for the case of a fiber with radius $a = 200$ nm, and a cesium atom probed at D2 line, $\lambda = 852$ nm, are investigated in [126]. The results are shown in the top plot of Fig. 2.2 g) for the transmittance, T, reflectance, R, and atomic decay rate ratio $\chi = \Gamma_p/\Gamma_0$ where Γ_p is the decay rate into the fiber mode ($\Gamma_p/2$ into the forward and backward directions each) and Γ_0 is the decay rate into the environment, taking into account the presence of the dielectric surface of the fiber. Note that all of the results are shown as dashed curves, with χ given by two curves representing the maximum and minimum for different magnetic sublevels [126].

Given the full calculation results taking into account many factors important in nano-waveguide systems [126], the goal now is to use this result as a basis to make estimations for similar systems in similar length scales. To check how close these estimates can be, we first would like to check them against the full calculation result itself. Our estimation procedure is the following: First we take the value for Γ_p at the surface of the (radius $a = 200$ nm) nanofiber, $\Gamma_{p,0} = (0.48 + 0.31)/2\gamma_0 = 0.395\gamma_0$,

which is computed using the full calculations in [126] for cesium D2 transition. The averaging gives the mean value across the range of $\Gamma_{\rm p}$ for different magnetic sublevels. Next, we know that $\Gamma_{\rm p} \sim \frac{1}{A_{\rm eff}}$, or equivalently we can write $\Gamma_{\rm p} = A_0 \frac{\lambda^2}{A_{\rm eff}}$ with A_0 a proportionality constant [42]. Note that λ^2 is just a normalization factor for the effective area $A_{\rm eff}$. At $\lambda = 852$ nm, this value is $A_0 = 0.16828$. Now independently, we can analytically calculate the effective area $A_{\rm eff}$ for a nanofiber with radius $a = 200$ nm, as a function of the atom-to-surface distance, d. The analytical equations describing a nanofiber mode and also the effective area are discussed in detail in Chapter 7. Given this function $A_{\rm eff}$ for this specific fiber geometry, we can then solve for the proportionality constant A_0 given the explicit value of $\Gamma_{\rm p,0}$. Next, we independently calculate the modification of the decay rate into the environment, Γ_0 (we used $\Gamma_{0\parallel}$) for a cesium atom near a silica dielectric surface, as discussed in Sec. 6.2.4.1 and shown in Fig. 6.1. With this, we plot the resulting (estimated) decay rate ratio $\chi = \Gamma_{\rm p}/\Gamma_0$, shown as the solid red curve in the top plot of Fig. 2.2 g). Finally, the transmittance T and reflectance R are given by [42, 41]:

$$T(\Gamma_{\rm p}, \Gamma_0, \Delta\omega) = \frac{\Gamma_0^2 + 4\Delta\omega^2}{(\Gamma_0 + \Gamma_{\rm p})^2 + 4\Delta\omega^2} \tag{2.29}$$

$$R(\Gamma_{\rm p}, \Gamma_0, \Delta\omega) = \frac{\Gamma_{\rm p}^2}{(\Gamma_0 + \Gamma_{\rm p})^2 + 4\Delta\omega^2}, \tag{2.30}$$

where $\Delta\omega = \omega - \omega_{\rm a}$ the detuning between the probe beam frequency ω and the atomic resonance frequency $\omega_{\rm a}$. In our calculations, we express $\Gamma_{\rm p}$ and Γ_0 in units of the free-space unmodified decay rate γ_0. The estimation results based on the aforementioned procedure are shown as solid curves in the top plot of Fig. 2.2 g) on resonant ($\Delta\omega = 0$). For comparison, we include the simple scattering ratio $R'_{\rm sc} = \sigma_0/A_{\rm eff}$ where $\sigma_0 = \frac{3\lambda^2}{2\pi}$ is the resonant absorption cross-section of an atom in free-space, where we see that this simple model for absorption ($1 - R'_{\rm sc} = P_{\rm T}/P_{\rm in} = T$) deviates significantly from the full-model T especially for decreasing atom-to-surface gap, d. We note that on resonant ($\Delta\omega = 0$), Eq. (2.29) and Eq. (2.30) reduce to:

$$T(\chi) = \frac{1}{(1+\chi)^2} \tag{2.31}$$

$$R(\chi) = \frac{\chi^2}{(1+\chi)^2}, \tag{2.32}$$

where $\chi = \Gamma_{\rm p}/\Gamma_0$ is the ratio of the decay rate into the chosen 'good' photonic mode to the decay rate into the environment (irreversible dissipation rate), $T = P_{\rm T}/P_{\rm in}$ is the transmittance, and $R = P_{\rm R}/P_{\rm in}$ is the reflectance.

As shown in the top plot of Fig. 2.2 g), although there is a slight deviation between the aforementioned estimation procedure results to the full results of [126] for the case of a nanofiber with radius $a = 200$nm, the estimates are good up to a few percent, and they are significantly different to the less precise simple model based on the simple scattering ratio $R'_{\rm sc} = \sigma_0/A_{\rm eff}$. Using the same estimation models and A_0 parameter as described above, we now change the effective area profile $A_{\rm eff} = A_{\rm eff}(d)$, for nanofibers with radius $a = 250$ nm, and $a = 215$ nm, which are the dimensions for the nanofiber atom trapping experiments in [248] and [91] respectively. The results are shown in the bottom plot of Fig. 2.2 g), where the bottom curves correspond to the [248] experimental parameters, and the top curves correspond to the [91] experimental parameters. The region in between the two curves is shaded for a visual guide. We note the deviations from the simple $R'_{\rm sc} = \sigma_0/A_{\rm eff}$ model are shown by the orange curves on the same plot. The points (i) and (ii) represent the experimental data of measurements of absorption, $1 - T$, for the two experiments, where atoms are located at the trap minima at $d = 230$ nm and $d = 215$ nm respectively. We see that the measured result of [91], point (ii), $(1 - T)_{\rm expt} = 0.0769$ (using single-atom optical depth $d_1 = 0.08$, and $T = e^{-d_1}$), is in a good agreement with the predicted value, $(1 - T)_{\rm pred} = 0.0838$. The measured result of [248], point (i), $(1-T)_{\rm expt} = 0.00648$ (using single-atom optical depth $d_1 = 0.0065$, and $T = e^{-d_1}$), is about a factor of seven smaller than the predicted value, $(1 - T)_{\rm pred} = 0.044$. As mentioned in [248], one factor that contributes to this difference is the inhomogeneous line broadening induced by the trapping light. Where this broadening is absent, the absorbance is estimated to increase by a factor of 2.5 [248].

Finally in Fig. 2.2 h), we present a contour plot of $\chi = \Gamma_{\rm p}/\Gamma_0$ as a function of $\lambda^2/A_{\rm eff}$ and d, the atom-to-surface distance, where we have used the values A_0 and $\lambda = 852$ nm as described above. We include in these contour plots the parameters corresponding to the experiments in [248] and [91] labeled (i) and (ii) respectively, where $(\lambda^2/A_{\rm eff}, d, \chi) = (0.1389, 230{\rm nm}, 0.0230)$ and $(0.2759, 215{\rm nm}, 0.045)$. The quantities $\lambda^2/A_{\rm eff}$ are calculated analytically using the model described in detail in Chapter 7. As discussed above, we note that while this prediction agrees with the experimental result of [91], point (ii), the prediction does not agree with the experimental result of [248]. One factor that causes this difference is the line broadening induced by the trapping light in [248] as discussed above.

The results of Fig. 2.2 h) may be used for other nanophotonic waveguides that may have different cross-sectional geometries such as a rectangle in a rectangular nanobeam, using the appropriate $A_{\rm eff}$ profiles that depend on the material refractive index and exact dimensions of the nano-waveguides.

Although it is less precise than using a full model approach such as with Green's functions [110], it is useful to give estimations and comparisons of the strength of atom-photon interaction in various nanophotonic waveguide designs. For the purpose of this section and in Fig. 2.1 e), we attribute a range of χ between 0 and 1 for nanophotonic waveguide systems discussed.

We note that there has been recent interest in investigations of nanophotonic waveguides that possess periodic structures that form band-structures [14, 159, 110]. In these systems, a large enhancement of the decay rate of the atom into the photonic crystal mode can be achieved by tuning the band-structure such that the frequency associated with the atomic resonant frequency corresponds to a small group velocity v_{g} of the photonic crystal mode. More precisely, the enhancement factor $\Gamma_{\mathrm{p}}/\Gamma_0$ is directly proportional to the inverse of the mode's group velocity v_{g}. These are discussed in detail in [159, 110]. For practically realizable structures, enhancement factors of ~ 10 are predicted, and an enhancement factor greater than 16 has been demonstrated in [14] at room temperature for a photonic crystal point defects slab containing a GaInAsP quantum well. For the purpose of this section, and in Fig. 2.1 e), we attribute an enhancement factor of up to 40 for waveguides with band structure relative to the range of $0 < \chi < 1$ for nanophotonic waveguides without any band-structure discussed in previous paragraphs. Hence, in Fig. 2.1 e), the range for χ for a nanoguide with band-structure is shown to be between zero and 40.

2.5.2 Atom-photon interactions within a cavity

As discussed in Sec. 2.4, a proven approach to achieve strong coupling between a single atom and a single photon is to use a high quality optical cavity, where a very high density of states for the atomic decay into the cavity mode compared to all other modes lost into the environment can be made very large, $\chi = \Gamma_{\mathrm{p}}/\Gamma_0 \ll 1$. Generic features of such a cavity QED system involve a high finesse ($\mathscr{F}$) optical cavity where photons can bounce inside the cavity mode for a large number of times, as well as a small cavity field mode volume (V_{m}) leading to high electric field intensity at the location of the atom from a single photon. In this section, we explore various cavity QED platforms including a microtoroidal cavity QED platform that is one of the focuses of this thesis, and look at the various key parameters including $Q, V_{\mathrm{m}}, C, \chi, |\vec{E}(\vec{r}_{\mathrm{a}})/\vec{E}_{\mathrm{max}}|$, as defined and discussed in Sec. 2.4, and illustrated in Fig. 2.3. We note that other parameters such as $\kappa, \kappa_{\mathrm{i}}, \kappa_{\mathrm{ex}}, g, \Gamma_{\mathrm{p}}, \Gamma_0, P_{\mathrm{in}}, P_{\mathrm{T}}, P_{\mathrm{T}}$, and d (the atom-to-surface distance) are defined in Sec. 2.4; please refer to this section for detailed information.

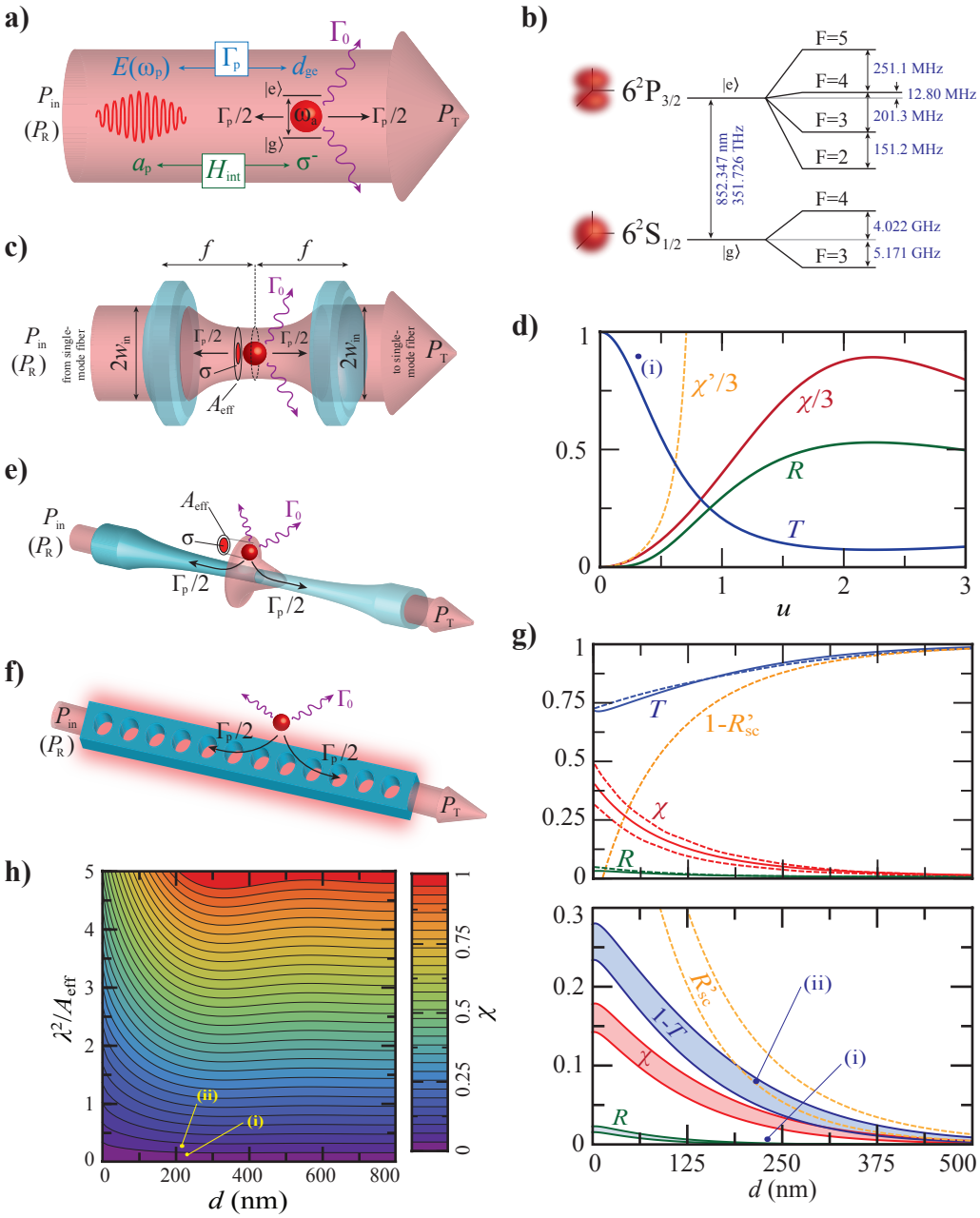

Figure 2.2: **Atom-photon interaction without a cavity.** **a,c,e,f)** Atom interacting with photonic mode a_p, $E(\omega_p)$ is the oscillating electric field at optical frequency ω_p; σ^- and d_{ge} are atomic lowering operator and electric dipole moment; H_{int}: atom-photon interaction Hamiltonian; P_{in}, P_R, P_T: input, reflected, transmitted optical power; Γ_p and Γ_0 are decay rate into photonic mode a_p and decay (loss) rate into the environment respectively; A_{eff} and σ are photonic effective area and atomic scattering cross-section respectively. **c)** f: focal length of the pair of lenses; w_{in}: input Gaussian beam waist (radius) size. **b)** Cesium D2 line energy levels/manifolds. **d,g,h)** T, R: transmittance and reflectance; $R_{Sc} = \sigma_0/A_{eff}$, atom scattering rate, where σ_0 is the atomic resonant scattering cross-section. **d)** Results for strongly focused light; χ: full model; χ': paraxial approximation; $u = w_{in}/f$, focusing strength; (i): Experimental result for T of [233]. **Top g)** Comparison between our approximate model (solid curves) and full results of [126] (dashed curves). **Bottom g)** Results using our model for parameters in [248] (fiber radius 250 nm) and [91] (fiber radius 215 nm) with measurements of $(1-T)$ shown by (i) and (ii) respectively. The variable d is the atom to fiber's surface distance. **h)** Contour plot of χ. Points (i) and (ii) correspond to parameters in [248] and [91] respectively. **g,h)** As evident in g), the prediction model agrees with [91], point (ii), but this is not the case for [248], point (i). This is discussed further in the text.

2.5.2.1 Fabry-Perot cavity

A Fabry-Perot cavity QED system is illustrated in Fig. 2.3 a), which consists of a pair of highly reflective mirrors with an atom positioned at the anti-node of the cavity's standing wave mode. We include the parameters achieved in the experiment described in [33, 131], where the reflectivity of each mirror is 0.999 998 4, giving a finesse $\mathscr{F} = 4.2 \times 10^5$, mirror radius of curvature = 0.2 m, cavity length of 44.6 μm, mode-volume of $V_{\rm m} = 3.0 \times 10^4 \sim 10^4$ μm^3, $\lambda = 852$ nm, quality factor of $Q = 2.2 \times 10^7 \sim 10^7$, and assuming that the atom is located (trapped) at the maximum electric field such that $|\vec{E}(\vec{r}_{\rm a})/\vec{E}_{\rm max}| = 1$. This leads to a coupling parameter $g/2\pi = 19$ MHz, $\kappa/2\pi = 4$ MHz, and $C = g^2/2\kappa\Gamma_{0\perp} = 23$ where $\Gamma_{0\perp} = \Gamma_0/2 = 2.61$ MHz. This set of parameters from the experiment in [33] is shown as the point a1 and line a1 in Fig. 2.3 parts e) and f) respectively. As in the Fabry-Perot cavity system, the atom is located far away from any dielectric surface, the spontaneous decay rate to the environment is given to a good approximation by the free-space decay rate $\Gamma_0 = \gamma_0$, and there is no dependence on the atom-to-surface gap parameter d as with other types of nanophotonic cavities discussed in later sections. We note that in a Fabry-Perot cQED system, the mirrors of the cavity have to be stabilized to within 0.01 picometers to maintain the cavity's resonance frequency relative to the atomic transition frequency [33].

Stronger atom-photon coupling has been achieved using Fabry-Perot cavity QED systems, for example in [107] with $g/2\pi = 110$ MHz, $\kappa/2\pi = 14.2$ MHz ($Q = 6 \times 10^6$), and $C = g^2/2\kappa\Gamma_{0\perp} = 163$ where $\Gamma_{0\perp} = \Gamma_0/2 = 2.61$ MHz. The ultimate limit due to a finite realistic $Q/V_{\rm m}$ ratio for a Fabry-Perot cavity QED system (taking into account the mirrors and dielectric layer coatings of the mirrors) as discussed in [106, 33] is $Q/V_{\rm m} \sim 10^{5.3}$ μm^{-3}, which gives an atom-photon cooperativity parameter of $C = 5000$ with $|\vec{E}(\vec{r}_{\rm a})/\vec{E}_{\rm max}| = 1$. This is shown as the point a2 and line a2 in Fig. 2.3 parts e) and f) respectively.

2.5.2.2 Microtoroidal cavity

A microtoroidal cavity QED system is illustrated in Fig. 2.3 b), which consists of a monolithic silica microtoroidal resonator that supports a circulating whispering gallery mode, which is optically coupled to a tapered optical nanofiber at a rate of $\kappa_{\rm ex}$. The total cavity Q includes both the intrinsic losses (due to material absorption, defect scatterrers and radiative losses) $\kappa_{\rm i}$ and extrinsic loss or input/output coupling rate $\kappa_{\rm ex}$, which is tunable by the positioning of the nanofiber relative to the toroid, which is discussed in more detail in Sec. 3.1.1.2. Note that the dominant source of intrinsic loss is absorption of silica material, which is orders of magnitude larger than the radiation loss for

typical toroid dimensions [224].

Due to its potential ultra high quality factors and small mode volumes, a microtoroidal cavity QED system is very attractive, allowing potentially strong atom-photon coupling even surpassing the practical limits of a Fabry-Perot cavity QED system. This, combined with the monolithic nature and scalability of its parallel lithographic fabrication [240] makes it a particularly promising platform for cavity QED.

In contrast to Fabry-Perot cavity systems, here an atom couples to the cavity mode via the evanescent field that extends $\sim \lambda/2\pi \sim 100$ nm away from the surface of the toroid. In this case, in addition to the spatially varying effective mode area $A_{\rm eff} = P_{\rm cav}/I_{\rm cav}(\vec{r})$ (where $P_{\rm cav}$ is the circulating power of the cavity, and $I_{\rm cav}(\vec{r})$ is the intensity profile of the cavity mode as a function of the coordinate $\vec{r}$), $\Gamma_{\rm p} = \Gamma_{\rm p}(\vec{r}_{\rm a})$, and $|\vec{E}(\vec{r}_{\rm a})/\vec{E}_{\rm max}|$, the decay rate into the environment, $\Gamma_0 = \Gamma_0(\vec{r}_{\rm a}) = \Gamma_0(d)$ also depends on the atom's location $\vec{r}_{\rm a}$ (see Fig. 5.1 (c)). Note that the distance d in this case is taken to be the atom-to-surface distance along the equatorial plane of the toroid ($z = 0$).

In Fig. 2.3 e), we include two experimental results of microtoroidal cavity QED experiments as described in [9] and [5], with the latter discussed in detail in Chapter 5. We calculate the parameters $A_{\rm eff} = P_{\rm cav}/I_{\rm cav}(\vec{r})$ and $|\vec{E}(\vec{r}_{\rm a})/\vec{E}_{\rm max}|$ by using finite element analysis software COMSOL. In the first case [9], the toroid's major diameter is $D_{\rm M} = 44$ μm and minor diameter is $D_{\rm m} = 6$ μm, giving a mode volume of $\sim 5 \times 100$ μm^3. Here, $\kappa/2\pi = 18$ MHz ($Q \approx 5 \times 10^6$) and $g/2\pi = 50$ MHz (inferred from measurements), corresponding to atoms located at ≈ 100 nm ($|\vec{E}(\vec{r}_{\rm a})/\vec{E}_{\rm max}| = 0.15$) from the toroid's surface. The cooperativity parameter is $C = 12$. The result of this experiment [9] is shown in Fig. 2.3 parts e) and f) as point b1 and curve b1 respectively, where in part f), we have taken into account the spatial variation of $\Gamma_{\rm p}(\vec{r}_{\rm a})$ through $A_{\rm eff}(\vec{r}_{\rm a})$ and $\Gamma_0 = \Gamma_0(\vec{r}_{\rm a})$ due to surface-modified spontaneous emission effects (see Sec. 6.2.4.1 and Fig. 6.1). For this particular case, we use $\Gamma_0(\vec{r}_{\rm a}) = \Gamma_{0\parallel}(d)$, for parallel atomic dipole orientation relative to the toroid's surface, assumed to be a flat plane.

Although the toroid's evanescent field extent has an exponential decay with decay constant $\lambda/2\pi$, which is sub-wavelength, the cross-sectional area of the mode is larger than in the case of nanophotonic waveguides such as nanofibers and nanobeams. As a result, the complex polarization properties associated with nanophotonic waveguides that involve significant longitudinal components of the electric field are not present in the case of the toroid. Here, we can use the simple formula for the scattering rate $R_{\rm sc} = \sigma_0/A_{\rm eff}$ where $\sigma_0 = 3\lambda^2/2\pi$ is the atomic resonant absorption cross-section

and $A_{\rm eff}(\vec{r}) = A_{\rm eff}(d)$ is the mode effective area. Using Eq. (2.29) and noting that $1 - T = R_{\rm sc}$, we have:

$$\chi = \frac{\Gamma_{\rm p}}{\Gamma_0} = \frac{R_{\rm sc} + \sqrt{1 - R_{\rm sc}} - 1}{1 - R_{\rm sc}}. \tag{2.33}$$

Now we consider the experimental parameters of [5]. The toroid's mode volume is about five times smaller than the case of [9]. Here, the toroid's major diameter is $D_{\rm M} = 22.5$ μm and minor diameter is $D_{\rm m} = 3$ μm, giving a mode volume of ~ 100 $\mu{\rm m}^3$. Here, $\kappa/2\pi = 20$ MHz ($Q \approx 10^7$) and $g/2\pi = 105$ MHz (inferred from measurements), corresponding to atoms located at ≈ 100 nm ($|\vec{E}(\vec{r}_{\rm a})/\vec{E}_{\rm max}| = 0.15$) from the toroid's surface. The cooperativity parameter is $C = 53$. The result of this experiment [5] is shown in Fig. 2.3 parts e) and f) as point b2 and curve b2 respectively. We note that in this experiment, we are able to detect strongly coupled single atoms in real time. The distribution of the atom-to-surface distance d has two peaks, one located at 100 nm and another at 200 nm (see Fig. 5.2 (c)). For atoms located at 200 nm from the surface, $g/2\pi = 52$ MHz and $C = 15$. For the overall ensemble average, $g/2\pi = 40$ MHz and $C = 8$.

Although the aforementioned microtoroid cavity QED experiments have already demonstrated quite strong atom-photon couplings, these are still orders of magnitude away from the projected limits of a microtoroid cQED system [224, 131]. It is projected that quality factors of $Q \sim 10^{10}$ and $Q \sim 10^{11}$ are realistically achievable. Using the same mode volume as above, $V_{\rm m} \sim 100$ $\mu{\rm m}^3$, this leads to a three to four order of magnitude increase in the $Q/V_{\rm m}$ ratios. This leads to cooperativity parameters $C \sim 10^4$ and $C \sim 10^5$. They are shown in Fig. 2.3 parts e) and f) as points b3-4 and curves b3-4 respectively.

Finally, we note that the points on the curves b1-4 in Fig. 2.3 f) correspond to the location d = 100 nm, which were experimentally accessed through measurements in the case for b1-2 [9, 5]. The decay rate ratio $\chi = \Gamma_{\rm p}/\Gamma_0$ is calculated by taking into account the enhancement of $\Gamma_{\rm p}$ due to the small $A_{\rm eff}$, multiplied by the enhancement of $\Gamma_{\rm p}$ due to the cavity effect; the Purcell factor $P_{\rm F} = 1 + 2C$; and the enhancement of Γ_0 due to the proximity of the atom to the dielectric surface, as calculated in Sec. 6.2.4.1. While the rest of the enhancement effects (factors) are in the order of ~ 1, the enhancement due to the cavity ranges from ~ 10 to $\sim 10^5$. As expected, this is the key quality of cavity QED that enables the atom-photon coupling strength to be orders of magnitude higher than similar systems without a cavity. This is enabled by the combination of high finesse (hence quality factor) and small mode volume.

2.5.2.3 Nanophotonic cavities

Figure 2.3 parts c) and d) illustrate nanophotonic waveguides (e.g., optical silica nanofiber, silicon nitride nanobeam) that may or may not have periodic structures (e.g., periodic holes), that may or may not have photonic crystal mirrors on both sides of the waveguide forming a cavity, and that may or may not have arrays of atoms, which can form mirrors and a one dimensional cavity.

We first consider the simple case of a bare silicon nitride nanobeam waveguide with none of the above features except a pair of photonic crystal mirrors on both sides of the waveguides, forming a cavity. Consider a set of currently realistic and readily achievable parameters, a nanobeam with rectangular cross-section width × height of 300 × 200 nm (the width is along the x axis and the height is along the y axis, see Fig. 3.11), and a cavity length of 100 μm. Given this, we roughly estimate a mode-volume of $V_{\rm m} \approx 20\ \mu{\rm m}^3$, i.e., $V_{\rm m} \sim 10\mu{\rm m}^3$. The pair of photonic crystal mirrors leads to a cavity linewidth of $\delta\omega \approx 20$ GHz (quality factor $Q \approx 17600$, i.e., $Q \sim 10^4$) and a finesse of $\mathscr{F} = 80$, i.e., $\mathscr{F} \sim 100$ (where we have used the group index $n_{\rm g} = 2.06$ as the effective refractive index[2], with $\lambda_0 = 852$ nm, the free-space wavelength). From COMSOL simulation, we estimate for this geometry that $|\vec{E}(d_x = 200{\rm nm}, y = 0)/\vec{E}_{\rm max}| = 0.3$, where the atom is located along the x-axis, at $d_x = 200$ nm away from the surface of the nanobeam, and for the nanobeam mode polarized along the x-axis. If the atom is located 200 nm away from the surface along the y-axis, $|\vec{E}(d_y = 200{\rm nm}, x = 0)/\vec{E}_{\rm max}| = 0.25$. It is also possible to have a double nanobeam waveguide, say with the same rectangular cross-sections, separated by 200 nm along the x-direction, and the atom symmetrically located at the center between the pair of nanobeams (see Fig. 3.13). In this case, the atom is located at 100 nm away from both surfaces on both sides, and $|\vec{E}(d_x = 100{\rm nm}, y = 0)/\vec{E}_{\rm max}| = 0.70$. Note that the electric field profiles of these nanobeams are discussed in more detail in Sec. 3.3. For completeness, we note that $|\vec{E}/\vec{E}_{\rm max}| = 0.33$ for a nanofiber waveguide (with fiber diameter 430 nm), with an atom located 215 nm away from the surface, in the same direction as the probe beam's linear polarization. For the purpose of Fig. 2.3 parts e) and f), we show the case for $|\vec{E}/\vec{E}_{\rm max}| = 0.70$ and $Q/V_{\rm m} = 10^3\ \mu{\rm m}^{-3}$ as point d1 and curve d1 in part e) and f) respectively. This leads to a cooperativity parameter of $C = 12$. Note that the cooperativity parameter C scales with the electric field strength at the atom location $\vec{r}_{\rm a}$ as $C \sim |\vec{E}(\vec{r}_{\rm a}/\vec{E}_{\rm max}|^2$.

[2]In this dispersive system, the effective refractive index is determined by the group index, $n_{\rm g} = c/v_{\rm g}$ where $v_{\rm g}$ is the group velocity. Using $n_{\rm eff} = \beta/k$, $\beta = n_{\rm eff}k = n_{\rm eff}\omega/c$, $\frac{d\beta}{d\omega} = \frac{1}{v_{\rm g}} = \frac{1}{c}\left(\omega\frac{dn_{\rm eff}}{d\omega} + n_{\rm eff}\right)$, the group index is given by $n_{\rm g} = \left(\omega\frac{dn_{\rm eff}}{d\omega} + n_{\rm eff}\right)$, where $n_{\rm eff}$ is the phase effective index (calculated for example by COMSOL), β is the guided mode propagation constant, and k is the free-space wave number. For our case of SiN nanobeam, with width $w =$ 300 nm, height $h = 200$ nm, we obtain from COMSOL, $n_{\rm eff} = 1.15 = \lambda_0/\lambda_{\rm cav}$. From COMSOL, we also obtain, by scanning the propagating optical angular frequency ω, the value $\frac{dn_{\rm eff}}{d\omega} = 3.90 \times 10^{-4}$ THz^{-1}.

The curve d1 in Fig. 2.3 f) shows $\chi = \Gamma_{\rm p}/\Gamma_0$, where $\Gamma_{\rm p} = \Gamma'_{\rm p} \times P_{\rm F}$ where $\Gamma'_{\rm p}$ is calculated taking into account the factors considered by the full model in Sec. 2.5.1.2 given by the solid curve χ in the top plot of Fig. 2.2 g), and $P_{\rm F}$ is the Purcell factor enhancement due only to the cavity. As with previous calculations, $\Gamma_0 = \Gamma_{0\|}$ is calculated according to Sec. 6.2.4.1 (see Fig. 6.1). The point on the curve d1 in Fig. 2.3 f) gives the specific atom-surface distance considered in the above paragraph, $d = 200$ nm.

The above parameters are calculated for a modest cavity finesse of $\mathscr{F} \approx 10^2$ ($Q \approx 10^4$) and a relatively large mode volume $V_{\rm m} \approx 10\ \mu{\rm m}^3$. One can imagine that the finesse of the photonic crystal cavities may be increased by a factor of 10 or 100 (keeping the mode volume constant), leading to an increase by a factor of 10 or 100 in Q. Alternatively, one can also reduce the mode volume by a factor of 10, say by reducing the cavity length by a factor of 10; in this case, the finesse needs to be increased by a factor of 10 in order to keep Q constant. Whichever the approach, or with the combined approach, we include in Fig. 2.3 e) and f) the points d2, d3 and curves d2, d3 respectively for the case where the ratio $Q/V_{\rm m}$ is increased by 10-fold and 100-fold. An estimate [224, 147] of the ultimate limit gives $Q/V_{\rm m} \approx 10^{6.5}\ \mu{\rm m}^{-3}$, leading to a cooperativity parameter of $C \approx 10^4$ (for $|\vec{E}/\vec{E}_{\rm max}| = 0.70$). This is included as point d4 and curve d4 in Fig. 2.3 e) and f).

At the end of Sec. 2.5.1.2, we discussed how periodic structure of nanophotonic waveguides may lead to band-structures that may be tailored to give a small group velocity of the mode, which may give further enhancement by a factor of ~ 10 for realistic fabrication parameters [110]. Using this technique, it may be possible to obtain a further enhancement say by 10-fold in the effective Q. This is surely highly simplified and is intended only to give rough order of magnitude estimates of the possible ranges. These cases are shown in Fig. 2.3 e) and f), labelled by d5, d6, d7, and d8. Here, we locate the atom right in the middle of the photonic crystal holes, such that $|\vec{E}/\vec{E}_{\rm max}| = 1$. As in this case, the behaviour of Γ_0 can deviate significantly from the other cases above, and we have set $\Gamma_0 = \gamma_0$, the free-space decay rate. We note that in this case, the largest projected limit can be $Q/V_{\rm m} = 10^{7.5}\ \mu{\rm m}^{-3}$ and have a cooperativity parameter of $C = 7 \times 10^5$, slightly higher than the 'ultimate limit' projected for a microtoroid cQED system ($C \approx 5 \times 10^5$ for an atom located at 150 nm away from the surface of the toroid).

Finally for completeness, we include in our comparisons the work of [41], which considers a new kind of cavity QED system where a one-dimensional linear array of atoms may be used to form a cavity surrounding a chosen/designated 'defect' atom. Here, it is predicted that a cooperativity parameter of $C \sim 10$ is achievable with $N_{\rm m} \sim 10^3$ number of mirror atoms surrounding the single

defect (qubit) atom, as illustrated in Fig. 2.3 c). Using $C = 10$ and $|\vec{E}/\vec{E}_{\max}| = 0.33$ (corresponding to the electric field of an atom located 215 nm away from a nanofiber of diameter 430 nm along the probe beam's linear polarization direction), we show in Figs. 2.3 e) and f), point c1 and curve c1. For the plot in part f), we have used the spatially dependent parameters $A_{\text{eff}}, \Gamma_{\text{p}}, \Gamma_0$ for a fiber of diameter 430 nm. We have also included as point c2 and curve c2, the case where $|\vec{E}/\vec{E}_{\max}| = 1$, which corresponds to $C \approx 90$.

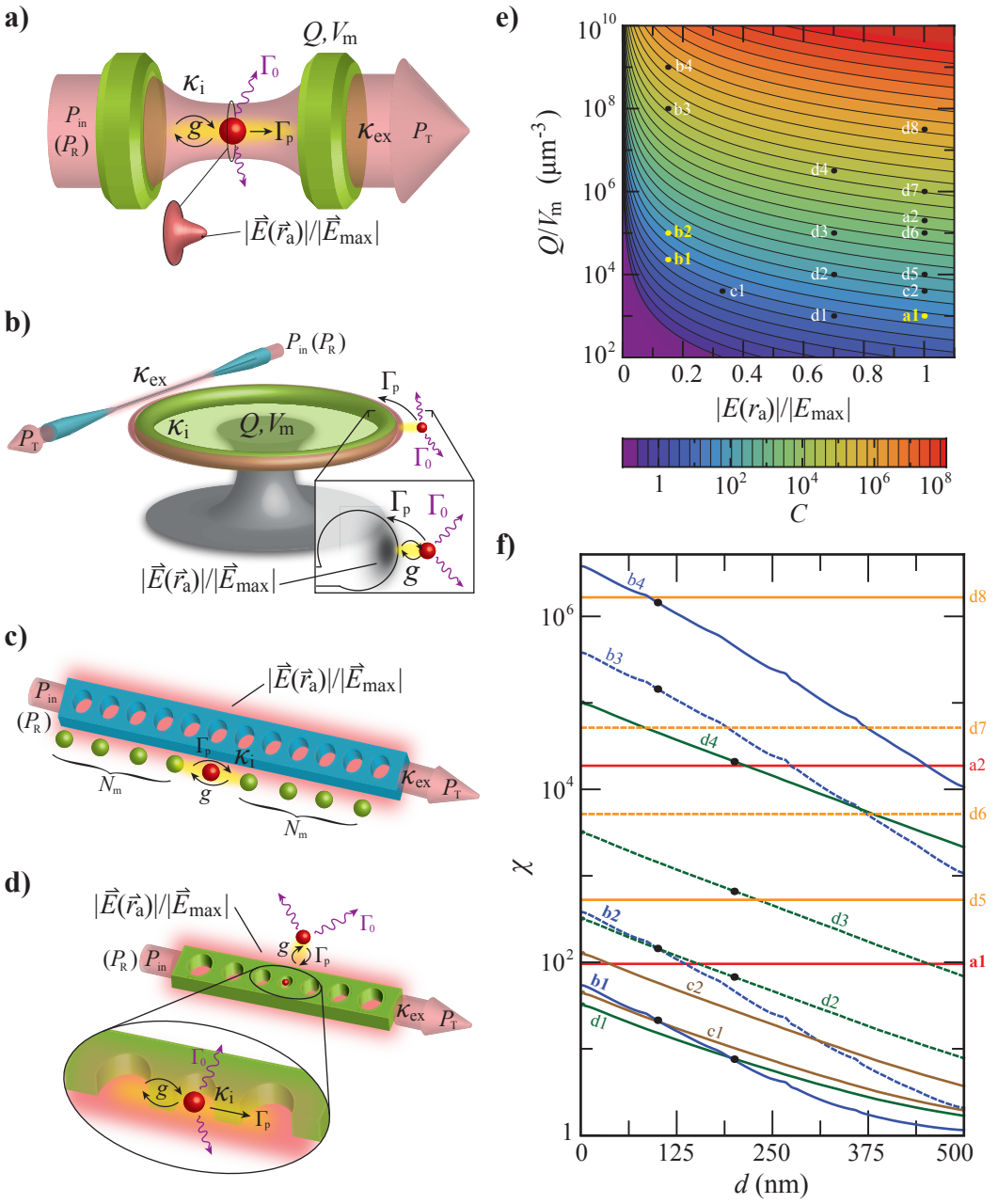

Figure 2.3: **Atom-photon interaction within a cavity.** **a,b,c,d)** Q: cavity quality factor, V_m: cavity mode volume; P_{in}, P_R, P_T: input, reflected, transmitted optical powers; g: atom-photon coupling rate; κ_i: intrinsic cavity loss; κ_{ex}: extrinsic input/output coupling rate; E_{max} and $E(\vec{r}_a)$ are the maximum electric field and the electric field at atom's position $\vec{r}_a$; Γ_p: atom's decay rate into cavity photonic mode; Γ_0: atom's decay rate into the environment. **e,f)** C: cooperativity parameter; $\chi = \Gamma_p/\Gamma_0$; d = atom-to-surface distance. **a)** Fabry-Perot cavity; labels in e) and f): a1, experimental parameters of [33], a2, ultimate limit [33]. **b)** Microtoroidal cavity; labels in e) and f): b1 and b2, experimental parameters of [9] and [5], b3 and b4, projected limits [224, 131]. **c)** Atomic mirror cavity (formed by 2 N_m atoms): c1, prediction from [41] with $|E|/|E_{max}| = 0.33$, c2, with $|E|/|E_{max}| = 1$. **d)** Photonic crystal cavity: d1-d4 for currently realizable Q/V_m value to the projected limit [147], with $|E|/|E_{max}| = 0.5$, d5-d8 for same range of Q/V_m but with $|E|/|E_{max}| = 1$ and an enhancement factor of 10 in atom's decay rate into the photonic mode that may be gained by utilization of photonic crystal band structure effect. Note: a1, a2, d5-d8 indicate values of χ (with $\Gamma_0 = \gamma_0$, the free-space decay rate), they are not functions of d. The horizontal lines serve as visual guides for comparison with other curves.